PHYSICAL REVIEW B **95**, 121405(R) (2017)

Current switching of electronic structures in two-dimensional 1*T*-TaS_2 crystals

Masaro Yoshida,[1,*] Takashi Gokuden,[1] Ryuji Suzuki,[1] Masaki Nakano,[1] and Yoshihiro Iwasa[1,2]

[1]*Department of Applied Physics and Quantum-Phase Electronics Center (QPEC), The University of Tokyo, Tokyo 113-8656, Japan*

[2]*RIKEN Center for Emergent Matter Science (CEMS), Wako 351-0198, Japan*

(Received 30 September 2016; revised manuscript received 20 February 2017; published 15 March 2017)

We report that a high electric field and current triggers the switching of multiple states in two-dimensional (2D) crystals of 1*T*-TaS_2, accompanying a metamorphosis of the electronic structure. We fabricated four-terminal devices of nanometer-thick crystals of 1*T*-TaS_2 with charge-density-wave (CDW) phases. By applying in-plane electric fields and concomitantly injecting currents, we realized nonvolatile switching among normal metals, Mott insulators, and thermally inaccessible semimetals. The field and current not only interact with the CDW but also generate Joule heat, and both effects contribute to the switching. The results indicate the potential existence of multiple electronic states accessible only in 2D crystals.

DOI: 10.1103/PhysRevB.95.121405

To search for memory functions and exotic electronic states, current switching phenomena have been intensively investigated in various systems [1–3], particularly oxide materials [4]. Here, caution should be taken to ensure that the switching is achieved only in extreme environments with high electric fields (on the order of kilovolts to megavolts per centimeter) and current densities (amperes to mega-amperes per centimeter squared) [1–5]. Such extreme situations are difficult to achieve in macroscopic bulk systems, but they are easily realized in nanometer-scaled devices because of their small volume [4,5]. Therefore, nanomaterials and their devices offer novel opportunities to observe dynamical switching and consequent peculiar states of matter.

We focus on a two-dimensional (2D) crystal: 1*T*-TaS_2 nanometer-thick crystals. Because of the quasi-2D Fermi surface owing to the layered structure [Fig. 1(a)], 1*T*-TaS_2 bulk crystals show successive charge-density-wave (CDW) phase transitions [6–8]. The ground state is a commensurate CDW (CCDW) phase, where 13 Ta atoms form a star-of-David cluster, as shown in Fig. 1(b). The electron at the central atom in the cluster is localized, leading to an insulating Mott state [9]. At room temperature, 1*T*-TaS_2 is in a hexagonal nearly commensurate CDW (NCCDW) phase consisting of insulating CCDW domains, which originate from beating of the periodicity of CDW and that of the underlying lattice [7]. At high temperatures, an incommensurate CDW (ICCDW) phase forms.

The electronic phases of nanometer-thick crystal devices are, however, significantly distinct from the thermal phases of bulk crystals. In thin crystal devices, the NCCDW-CCDW phase transition is absent and there is no large jump in the temperature-dependent resistivity curve [see Fig. 1(c)]. Instead, the supercooled NCCDW state persists to low temperatures. Reduction in the thickness always suppresses the CCDW ordering [10–13], indicating thinning-induced slow ordering kinetics [10,12,13]. Because of the slow ordering kinetics, the 2D 1*T*-TaS_2 crystals are platforms to search for metastable electronic phases. In thin crystals, switching to metastable states can be achieved by applying high in-plane electric fields accompanying large current flows [12–16], and a schematic of the measurement setup is shown in Fig. 1(d). The application of high electric fields induces the switching not only to CCDW/NCCDW/ICCDW phases [12–16] but also to thermally inaccessible phases [12,15]. Hence, the energy landscape for the thin crystals has many potential minima. In this Rapid Communication, we attempted to induce multiple states in thin crystal devices, and clarify the effect of the field and current on the electronic structure.

First, we performed switching at various temperatures. We cooled a 19-nm-thick crystal from 370 K to a certain temperature to set the system in the NCCDW phase. We then swept the in-plane electric field (E) at a scanning rate of 18 $\mathrm{V\,cm^{-1}\,s^{-1}}$.

The switching operation strongly depends on the temperature at which the electric field is applied. At 90 K, one E scan caused an increase in the sheet resistance (R_s) [see Fig. 2(a)], and its repetition gradually increased R_s. This memristive switching occurs from a supercooled NCCDW state to the thermodynamically stable CCDW phase, and is attributed to Joule heating by the current flow [12]. The Joule heating effect enhanced the growth of insulating CCDW domains, and consequently increased R_s. The switching operation at higher temperatures was qualitatively different from that at 90 K. An example is shown by the red normalized R_s-E curve in Fig. 2(b) obtained at 225 K, exhibiting both volatile and nonvolatile switching with hystereses. Volatile switching was accompanied by a hysteresis at $5.7 \leqslant E \leqslant 6.0\,\mathrm{kV\,cm^{-1}}$, and nonvolatile switching was accompanied by a hysteresis at $0 \leqslant E \leqslant 1.8\,\mathrm{kV\,cm^{-1}}$.

Volatile switching has a clear threshold electric field (E_{th1}, $6.0\,\mathrm{kV\,cm^{-1}}$ for switching at 225 K), where R_s suddenly decreases and becomes constant with increasing E. Because the constant value of R_s is almost equal to that of the ICCDW phase at 370 K, volatile switching is a phase transition to the ICCDW phase.

On the other hand, nonvolatile switching has two characteristic electric fields of E_{th2} and E_{th3} (0.84 and $1.8\,\mathrm{kV\,cm^{-1}}$ for switching at 225 K, respectively). At 225 K, R_s is almost constant at $0 \leqslant E < E_{th2}$ and starts to decrease at E_{th2} with increasing E, followed by the closing of the hysteresis at E_{th3}. Because of the broad nature of the switching, we defined E_{th2} as the E value where the two dashed lines cross [see the two light-blue dashed lines in Fig. 2(b)], and E_{th3} as

*masaro-yoshida@mp.t.u-tokyo.ac.jp

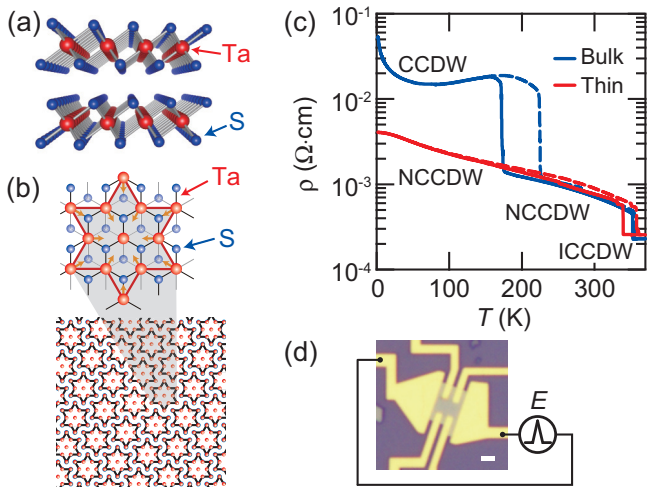

FIG. 1. (a) Crystal structure of $1T$-TaS_2. (b) Star-of-David clusters in the CCDW phase. (c) ρ-T curves for bulk (thickness, $t = 300\,\mu$m) and thin ($t = 24$ nm) single crystals. The solid and dashed lines are the data obtained with decreasing and increasing temperature, respectively. (d) Optical micrograph of a thin crystal device (scale bar 1 μm).

the E value where dR_s/dE is minimum in the forward scan. Upon increasing E, the system is in the initial NCCDW state at $0 \leqslant E < E_{th2}$ and in the final metastable state at $E_{th3} < E < E_{th1}$, whereas it is in an intermediate state at $E_{th2} < E < E_{th3}$. We henceforward refer to the E-triggered final state as NCCDW*.

We use the definition of E_{th2} and E_{th3} to obtain the threshold electric fields at each temperature. Figure 2(c) is the summarized T vs E phase diagram, where E_{th1}, E_{th2}, and E_{th3} are represented by red, light-blue, and dark-blue symbols, respectively.

In Fig. 2(c), E_{th1} saturates with decreasing temperature, which is consistent with other reports [14,16]. Because the ICCDW phase is thermally accessible, it is natural to attribute the phase transition to Joule heating. On the other hand, E_{th2} rapidly increases with decreasing temperature. As represented by the straight black dashed line in Fig. 2(c), E_{th2} seems to obey the following temperature dependence, $E_{th2}(T)/E_{th2}(0) = \exp(-T/T_0)$. The exponential T dependence in CDW systems is interpreted as the weakening of the pinning potential due to the thermal fluctuation of the CDW phase [17]. The results suggest that the switching to the NCCDW* state is triggered by the depinning of the CDW. The sliding of the CDW stops at E_{th3}, indicating that the sliding realizes a new configuration of the CDW and lattice whose energy has a local minimum in the complex energy landscape of the 2D $1T$-TaS_2 crystal. The values of $E_{th2}(10^2$-10^4 V cm$^{-1})$ are much larger than the typical values of the threshold field (10^{-2}-10^{-1} V cm^{-1}) for conventional ICCDW pinned by impurities. The high E_{th2} reflects the peculiar nature of the initial NCCDW state, where

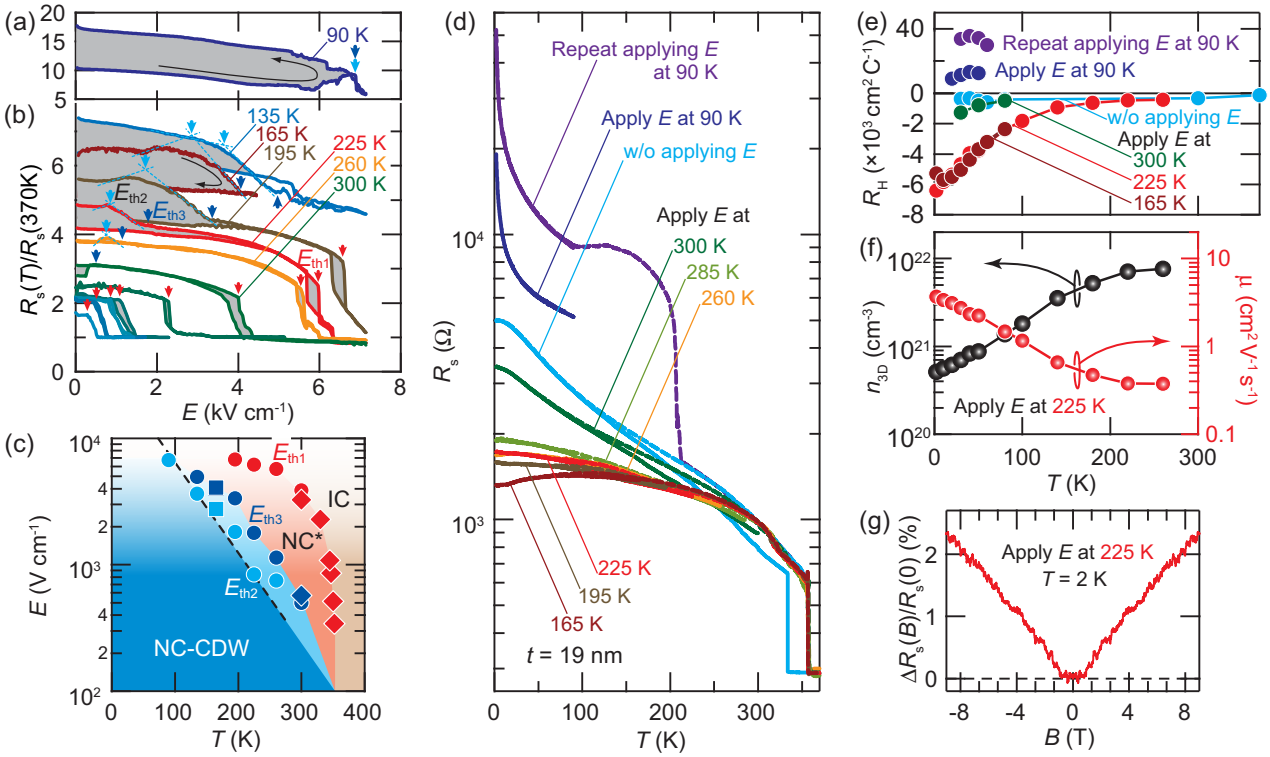

FIG. 2. (a), (b) Normalized R_s [$R(T)/R(370\,\text{K})$] vs E curves for 19-nm-thick crystal devices measured at (a) 90 K and (b) higher temperatures. From top to bottom, the T's are 90, 135, ..., 300, 330, 345, 347, 350, and 352 K. Sweep rate 18 V cm^{-1} s^{-1}. The red, light-blue, and dark-blue arrows represent the values of E_{th1}, E_{th2}, and E_{th3}, respectively. (c) T dependence of threshold electric fields from the three different samples, each marked with a differently shaped solid symbol. (d), (e) T dependence of (d) R_s and (e) R_H for a crystal measured with different temperatures to apply E's. (f) T dependence of n_{3D} (left ordinate) and μ (right ordinate) for the crystal switched at 225 K. (g) MR at 2 K for the crystal switched at 225 K.

the CDW is periodically pinned by the underlying lattice commensurability.

After switching, we cooled the sample to 2 K. Figure 2(d) shows the R_s-T curves measured with different temperatures to apply the in-plane electric fields. The top purple and dark-blue lines are the R_s-T curves that were obtained after scanning E several times and once at 90 K, respectively. Their insulating behavior is characteristic of the CCDW-Mott phase. The light-blue R_s-T curve represents the supercooled NCCDW state that was obtained without applying an in-plane electric field. In contrast to the CCDW and NCCDW states, the multiple NCCDW* states triggered at $T \geqslant 165$ K were more conducting at low temperatures. Upon warming, the R_s-T curves for the switched sample finally coincided with the initial curve obtained without applying an in-plane electric field. This recovery to the NCCDW and ICCDW phases indicates the metastability of the E-triggered NCCDW* conducting states. The multiple R_s-T curves in Fig. 2(d) confirm the existence of various thermally inaccessible metastable NCCDW* states that are evoked by applying in-plane electric fields.

Figure 2(e) shows the temperature dependence of the Hall coefficient (R_H), which provides important insight into the electronic structure. The insulating states have large positive R_H values ($>1 \times 10^4$ cm^2 C^{-1}), which proves the thermal equilibrium state of the CCDW phase [18]. For the supercooled NCCDW state, R_H shows almost temperature-independent behavior ($|R_H| < 5 \times 10^2$ cm^2 C^{-1}), which reflects the normal metallic character of the NCCDW phase and is consistent with angle-resolved photoemission measurements capturing the Fermi surface around the Γ point in the NCCDW phase [19].

In contrast, for the conducting NCCDW* state, the absolute value of R_H dramatically increases with decreasing temperature. Because transverse resistance (R_{xy}) was linearly dependent on the magnetic field (B) from 0 to 9 T, we use the single-carrier Drude band model to calculate the carrier density [$n_{3D} = 1/(etR_H)$] and mobility ($\mu = R_H/R_s$), where e is the elementary charge and t is the thickness. As shown in Fig. 2(f), the electron carrier concentration (n_{3D}) is found to be 5×10^{20} cm^{-3} at 2 K in the sample switched at 225 K (there are 0.03 electrons per Ta atom at 2 K), and increases slowly with temperature, exhibiting semimetal-like or small-gap-like behavior. Figure 2(f) also shows that the electron mobility monotonically increases with decreasing temperature in the NCCDW* state. The observed decrease in n_{3D} and increase in μ upon cooling are the characteristics of semimetals or zero-gap conductors [20–22]. Furthermore, in the switched state, we observed a magnetoresistance (MR) $\{\Delta R_s(B)/R_s(0) = [R_s(B) - R_s(0)]/R_s(0)\}$ that is linear rather than parabolic [see Fig. 2(g)]. Such a linear MR is reminiscent of a semimetal whose conduction-band bottom and valence-band top touch at the same point in momentum space, including zero-gap topological insulators [22–24] and Dirac semimetals [25]. By considering the peculiar features mentioned above, we can regard the E-triggered metastable state as a semimetal. The relatively high n_{3D} indicates that the E-induced semimetal is heavily doped with electrons, which explains the small MR and the linear $R_{xy}(B)$. We conclude that the change in the switching temperature produced various material phases with different band topologies, from the supercooled NCCDW metal, to the CCDW-Mott insulator, to the metastable NCCDW* semimetal.

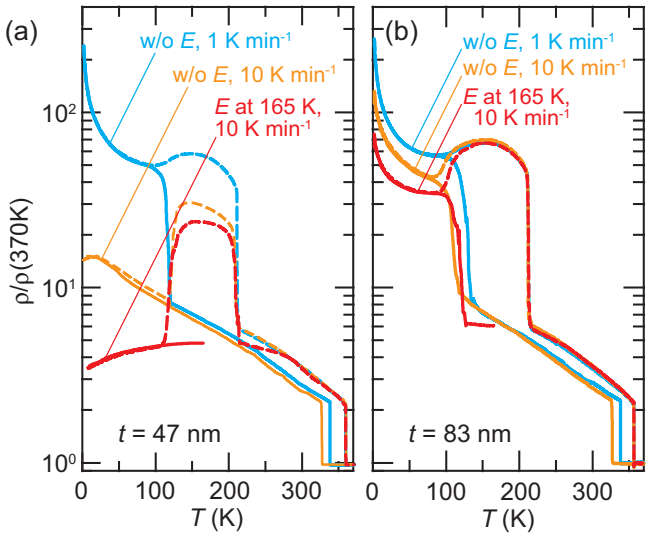

FIG. 3. (a) Normalized ρ [ρ/ρ(370 K)] vs T curves for (a) 47-nm- and (b) 83-nm-thick crystals. Light-blue curve: cooled and warmed at 1 K min^{-1} without switching. Yellow curve: cooled at 10 K min^{-1} and warmed at 1 K min^{-1} without switching. Red curve: switched at 165 K, cooled at 10 K min^{-1}, and warmed at 1 K min^{-1}.

To assess the universality of the E-triggered metastable semimetallic NCCDW* states, we performed switching for thicker samples. We first prepared a 47-nm-thick crystal, whose NCCDW-CCDW transition can be suppressed by rapid cooling at 10 K min^{-1} [see the light-blue and yellow curves in Fig. 3(a)]. We applied an in-plane electric field at 165 K, and a metastable NCCDW* state was realized at low temperatures by quick cooling [see the red curve in Fig. 3(a)]. We then prepared an 83-nm-thick crystal, which is sufficiently thick to undergo a NCCDW-CCDW transition even with rapid cooling at 10 K min^{-1} [see Fig. 3(b)]. We performed switching at 165 K and cooled the crystal at 10 K min^{-1}. Until the transition to the CCDW phase occurred, we encountered a peculiar ρ-T curve with a weak T dependence, which is a clear sign of the E-triggered metastable semimetallic nature. Therefore, the semimetallic state is inherent even in bulk 1T-TaS_2 crystals, although it cannot be stabilized down to low temperatures. The results also emphasize the importance of thinning-induced slow ordering kinetics to stabilize the E-triggered metastable state.

Because an E-triggered semimetallic NCCDW* state can exist even in thick crystals, research on phase control in bulk crystals should provide insight into the NCCDW* states in 2D 1T-TaS_2 crystals. It has been reported that the introduction of disorder or defects suppresses the NCCDW-CCDW transition in bulk crystals [26]. In bulk crystals with disorder or defects, angle-resolved photoemission [19,27] and scanning tunneling spectroscopy [28–30] measurements revealed a reduction in the Mott gap and an emergence of a metallic phase. The ρ-T curve of the disordered bulk systems has been reported to be that of an insulator [26,27] or a quenched NCCDW state [19,26].

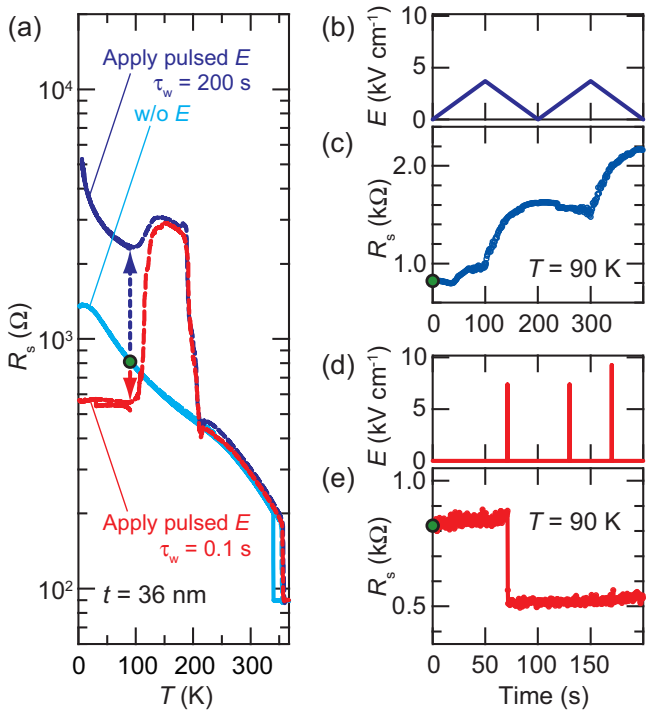

FIG. 4. (a) R_s-T curves obtained after switching at 90 K for a 36-nm-thick crystal. Light-blue curve: cooled without switching. Dark-blue curve: applied a pulsed E with $\tau_w = 200$ s twice at 90 K. Red curve: applied pulsed E's with $\tau_w = 0.1$ s. (b)–(e) Time evolution of E and R_s measured with (b), (c) $\tau_w = 200$ s and (d), (e) $\tau_w = 0.1$ s.

The electronic structure of the E-triggered NCCDW* state can be similar to that of the disordered systems, because a reduction in the Mott gap at the Γ point can result in a very small overlap of the upper and lower Hubbard bands and provide a semimetal-like band structure at the Γ point. However, the NCCDW* states in thin crystals exhibit a positive temperature coefficient of resistivity in a wide temperature range [Figs. 2(d) and 3(a)], which has yet to be observed in bulk crystals with disorder. Further research is necessary to elucidate the structure of the NCCDW* state and the origin of its semimetallic nature.

Finally, we investigated the duration time dependence of the switching to create functionalities. We prepared a 36-nm-thick crystal device and set the temperature at 90 K to realize the supercooled NCCDW state [see the light-blue R_s-T curve in Fig. 4(a)]. As shown in Fig. 4(b), we first applied triangular-shaped electric pulses with a long duration time (τ_w) of 200 s. We then observed a steplike change in R_s, as shown in Fig. 4(c). This memristive switching results from the growth of CCDW domains by Joule heating. The high-resistance state realized after switching was confirmed to be the CCDW phase, as indicated by the insulating R_s-T curve in Fig. 4(a). Figures 4(d) and 4(e) show that R_s abruptly decreases upon applying a short pulsed in-plane electric field with $\tau_w = 0.1$ s. The resulting R_s-T curve is represented by the red curve in Fig. 4(a), and a metastable semimetallic NCCDW* state was evoked. Because a short duration time corresponds to small Joule heat, the growth of CCDW domains was inhibited during application of the in-plane electric field, and the interaction between CDW and E was dominant in the switching operation. Here, we can dynamically change the state of matter by just changing the duration time.

We would like to acknowledge discussions with F. Kagawa. This work was supported by Grants-in-Aid for Scientific Research (Grants No. 25000003 and No. 25708040) from the Japan Society for the Promotion of Science (JSPS). M.N. was partly supported by a Grant for Basic Science Research Projects from the Sumitomo Foundation. M.Y. and R.S. were supported by JSPS through a research fellowship for young scientists.

[1] T. W. Hickmott, J. Appl. Phys. **33**, 2669 (1962).
[2] R. S. Potember, T. O. Poehler, and D. O. Cowan, Appl. Phys. Lett. **34**, 405 (1979).
[3] A. Asamitsu, Y. Tomioka, H. Kuwahara, and Y. Tokura, Nature (London) **388**, 50 (1997).
[4] A. Sawa, Mater. Today **11**, 28 (2008).
[5] J. J. Yang, D. B. Strukov, and D. R. Stewart, Nat. Nanotechnol. **8**, 13 (2013).
[6] T. Ishiguro and H. Sato, Phys. Rev. B **44**, 2046 (1991).
[7] R. E. Thomson, B. Burk, A. Zettl, and J. Clarke, Phys. Rev. B **49**, 16899 (1994).
[8] A. Spijkerman, J. L. de Boer, A. Meetsma, G. A. Wiegers, and S. van Smaalen, Phys. Rev. B **56**, 13757 (1997).
[9] P. Fazekas and E. Tosatti, Physica B+C **99**, 183 (1980).
[10] M. Yoshida, Y. J. Zhang, J. T. Ye, R. Suzuki, Y. Imai, S. Kimura, A. Fujiwara, and Y. Iwasa, Sci. Rep. **4**, 7302 (2014).
[11] Y. Yu *et al.*, Nat. Nanotechnol. **10**, 270 (2015).
[12] M. Yoshida, R. Suzuki, Y. J. Zhang, M. Nakano, and Y. Iwasa, Sci. Adv. **1**, e1500606 (2015).
[13] A. W. Tsen *et al.*, Proc. Natl. Acad. Sci. USA **112**, 15054 (2015).
[14] M. J. Hollander, Y. Liu, W. J. Lu, L. J. Li, Y. P. Sun, J. A. Robinson, and S. Datta, Nano Lett. **15**, 1861 (2015).
[15] I. Vaskivskyi, I. A. Mihailovic, S Brazovskii, J. Gospodaric, T. Mertelj, D. Svetin, P. Sutar, and D. Mihailovic, Nat. Commun. **7**, 11442 (2016).
[16] G. Liu, B. Debnath, T. R. Pope, T. T. Salguero, R. K. Lake, and A. A. Balandin, Nat. Nanotechnol. **11**, 845 (2016).
[17] K. Maki, Phys. Rev. B **33**, 2852 (1986).
[18] R. Inada, Y. Onuki, and S. Tanuma, Phys. Lett. A **69**, 453 (1979).
[19] F. Zwick, H. Berger, I. Vobornik, G. Margaritondo, L. Forro, C. Beeli, M Onellion, G. Panaccione, A. Taleb-Ibrahimi, and M. Grioni, Phys. Rev. Lett **81**, 1058 (1998).
[20] C. Shekhar *et al.*, Nat. Phys. **11**, 645 (2015).
[21] K. Kajita, Y. Nishio, N. Tajima, Y. Suzumura, and A. Kobayashi, J. Phys. Soc. Jpn. **83**, 072002 (2014).
[22] C. Shekhar, S. Ouardi, A. K. Nayak, G. H. Fecher, W. Schnelle, and C. Felser, Phys. Rev. B **86**, 155314 (2012).

[23] R. Xu, A. Husmann, T. F. Rosenbaum, M. L. Saboungi, J. E. Enderby, and P. B. Littlewood, Nature (London) **390**, 57 (1997).
[24] X. Wang, Y. Du, S. Dou, and C. Zhang, Phys. Rev. Lett. **108**, 266806 (2012).
[25] T. Liang, Q. Gibson, M. N. Ali, M. Liu, R. J. Cava, and N. P. Ong, Nat. Mater. **14**, 280 (2014).
[26] H. Mutka, L. Zuppiroli, P. Molinie, and J. C. Bourgoin, Phys. Rev. B **23**, 5030 (1981).
[27] E. Lahoud, O. N. Meetei, K. B. Chaska, A. Kanigel, and N. Trivedi, Phys. Rev. Lett. **112**, 206402 (2014).
[28] D. Cho, Y. H. Cho, S. W. Cheong, K. S. Kim, and H. W. Yeom, Phys. Rev. B **92**, 085132 (2015).
[29] D. Cho, S. Cheon, K. S. Kim, S. H. Lee, Y. H. Cho, S. W. Cheong, and H. W. Yeom, Nat. Commun. **7**, 10453 (2016).
[30] L. Ma *et al.*, Nat. Commun. **7**, 10956 (2016).